Krey et al., https://doi.org/10.1083/jcb.201606036

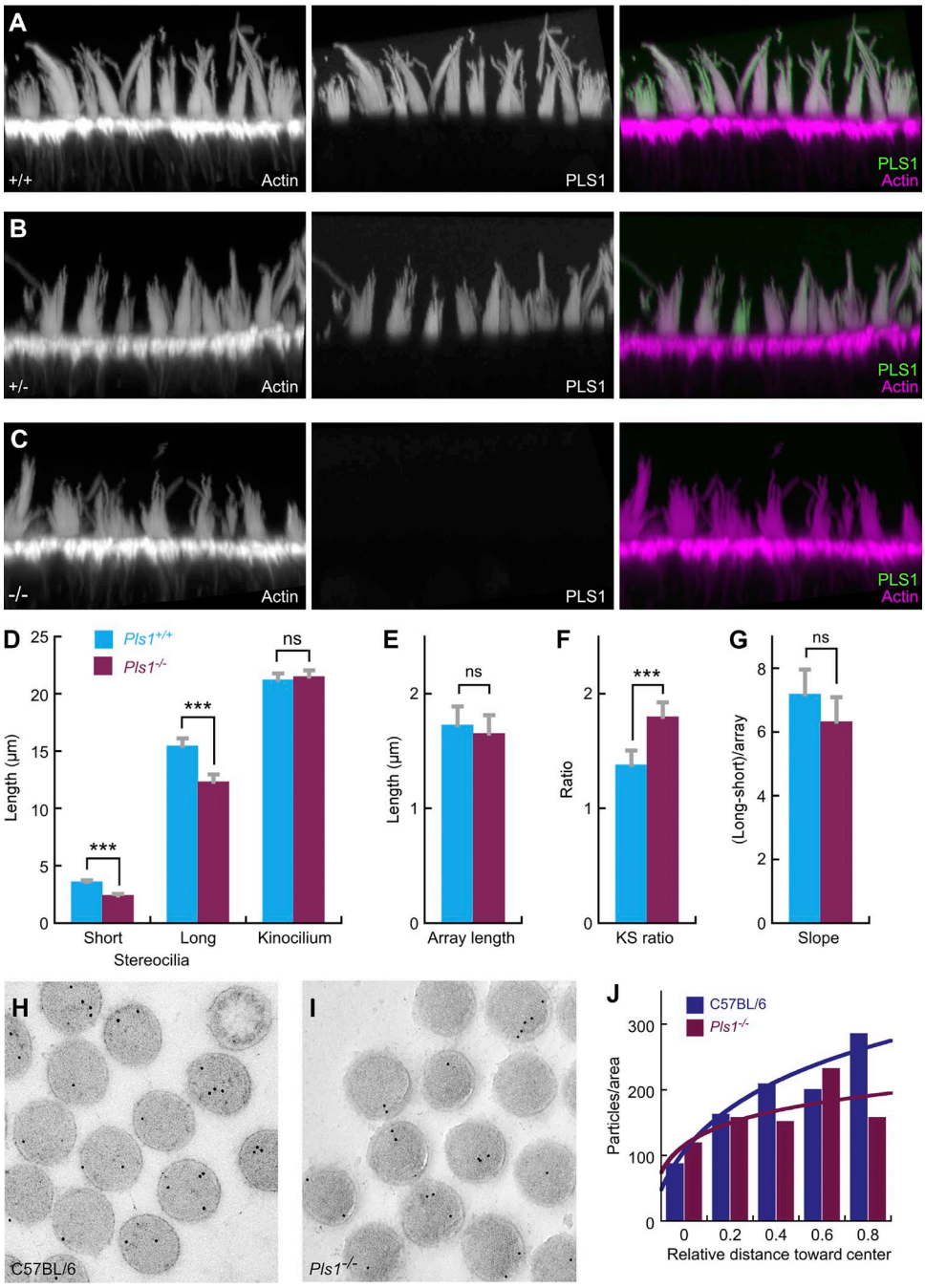

Figure S1. **Characterization of stereocilia in *Pls1*$^{-/-}$ mice.** (A–C) Labeling of utricle hair cells with Alexa Fluor 488–labeled anti-PLS1. Panels are 54 µm wide. (A) Wild-type littermate (*Pls1*$^{+/+}$). (B) Heterozygote (*Pls1*$^{+/-}$). (C) Homozygote null (*Pls1*$^{-/-}$). (D–G) Hair bundle morphology parameter values. Mean ± SEM are plotted. We measured several previously described parameters that describe the dimensions of hair bundles (Li et al., 2008), including the heights of the tallest and shortest stereocilia (D), the kinocilium height (D), and the array length (E), which is the distance from the tallest to the shortest stereocilia, measured parallel to the hair cell's apical surface. We used these measurements to calculate a KS ratio (F), which is the height of kinocilium divided by the height of the tallest stereocilia, and the bundle slope (G), which is the height of tallest stereocilia minus the height of the shortest stereocilia, divided by the array length. ***, $P < 0.001$. (H–J) Immunogold electron microscopy analysis of utricle stereocilia from C57BL/6 and *Pls1*$^{-/-}$ mice. (H) Labeling of C57BL/6 with anti-ESPN. (I) Labeling of *Pls1*$^{-/-}$ with anti-ESPN. Panels in H and I are 1,070 nm wide. (J) Immunogold density analysis. Gold particles were counted from concentric rings (bins) corresponding to 0.2× radius. Using a χ^2 test with p-values based on simulations, $P = 0.40$ for the C57BL/6 to *Pls1*$^{-/-}$ comparison. To display the density, the number of gold particles in a ring was divided by the ring's area and plotted against the distance to the center of the stereocilium. Using the relative distances, a Kolmogorov–Smirnov nonparametric test indicates $P = 0.59$.

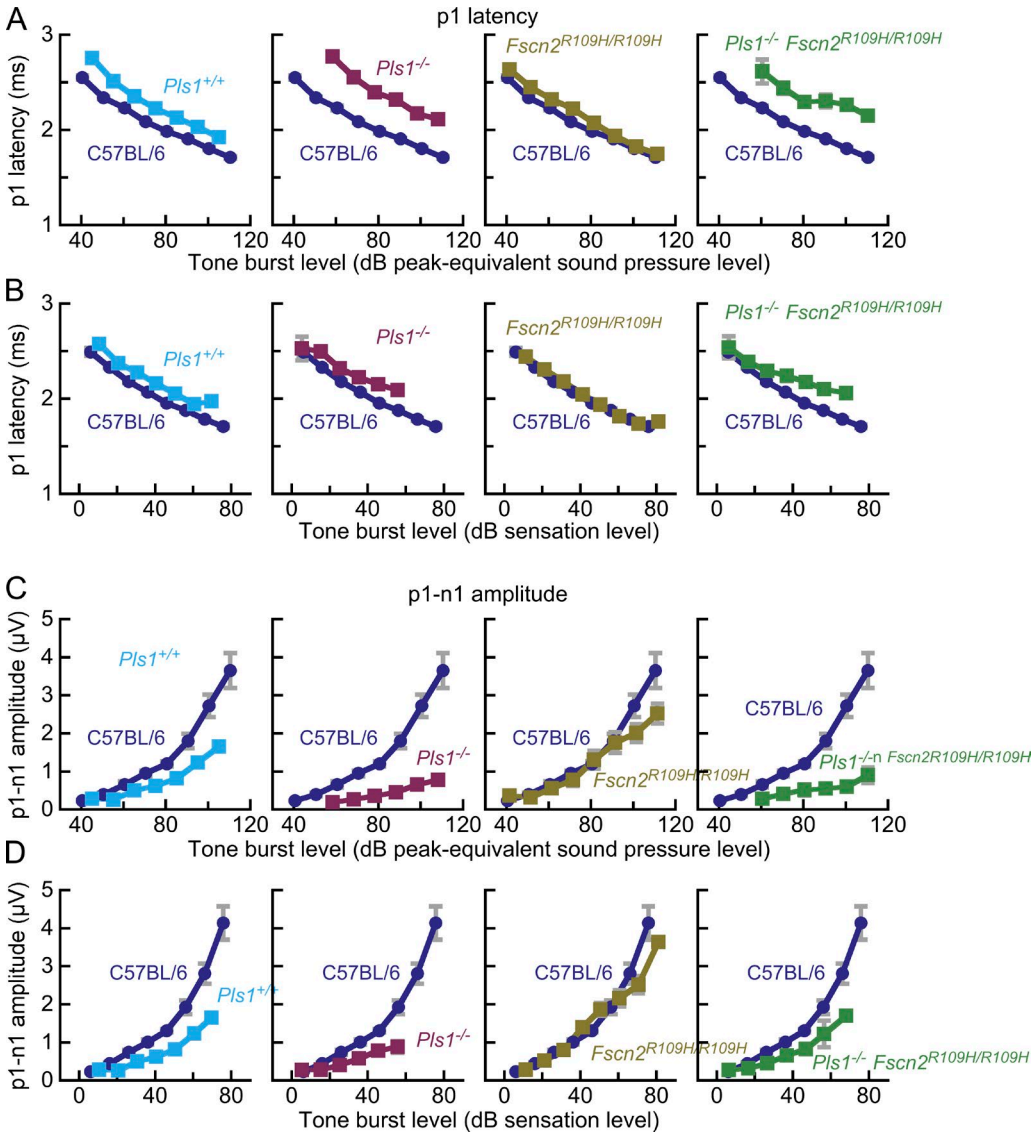

Figure S2. **Latencies and amplitudes for ABRs at 8 kHz.** All animals were 2 mo old. For each set, the x axis for the top panels is the absolute stimulus level. (A and B) p1 latencies. In A, the x axis for the top panels is the absolute stimulus level. In B, the x axis represents stimulus level normalized for threshold, where 0 dB represents each animal's ABR threshold and increasing values represent sound levels above threshold. (C and D) p1-n1 amplitudes. C shows absolute levels and D shows normalized levels. When normalized for threshold, the latency-intensity and amplitude-intensity functions essentially overlapped across genotypes; this result suggests that the differences in latency and amplitude between the genotypes are caused by the sensitivity of the cochlea rather than characteristics of the auditory nerve or brainstem auditory activity. Mean ± SEM are plotted for each point.

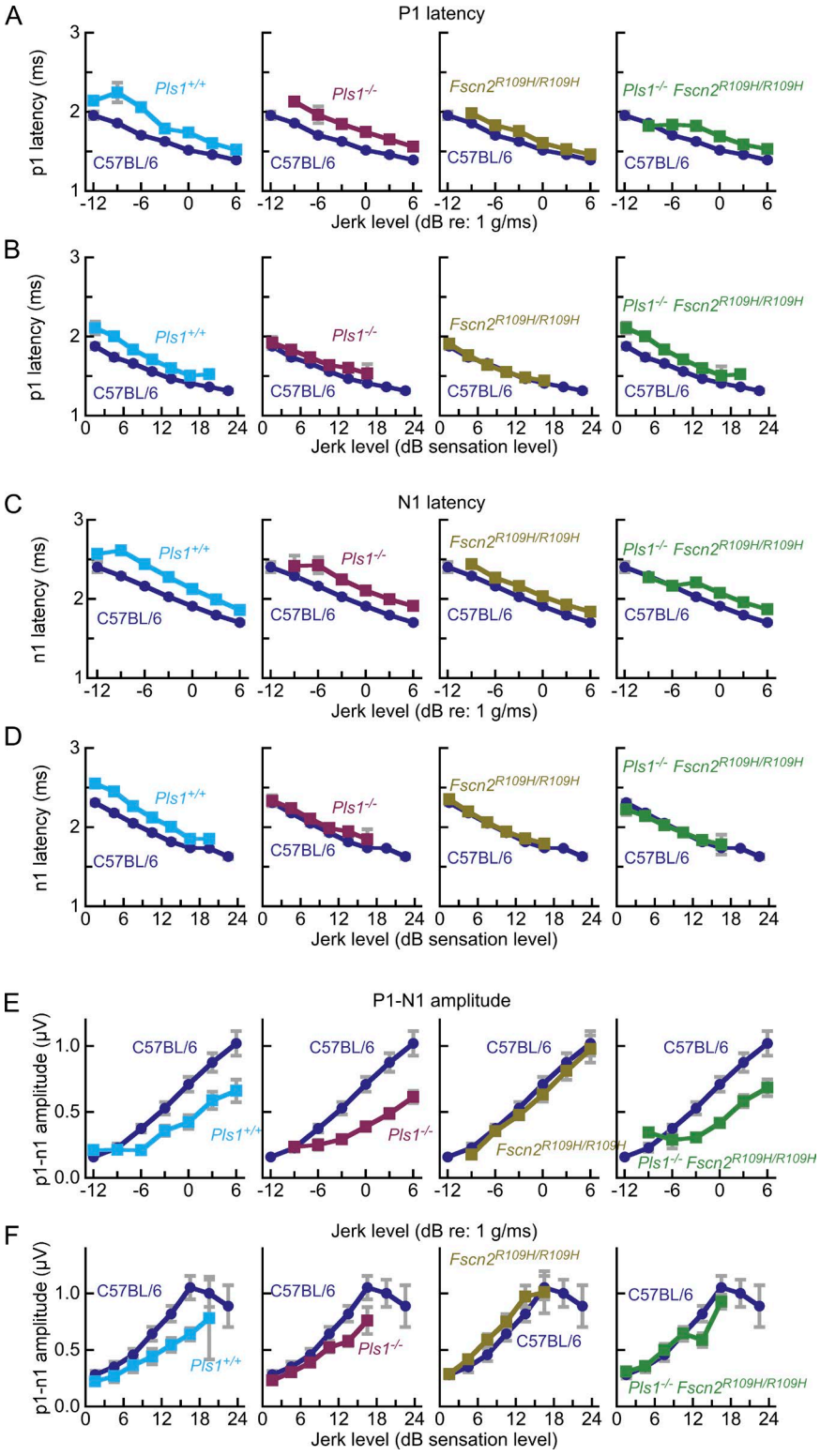

Figure S3. **Latencies and amplitudes for vestibular evoked potentials.** All animals were 2 mo old. As in the previous figure, for each set, the x axis for the top panel (A, C, and E) is the absolute stimulus level, and the x axis in the bottom panel (B, D, and F) represents stimulus level normalized for threshold, where 0 dB represents each animal's VsEP threshold and increasing values represent levels of head motion above threshold. (A and B) p1 latencies. (C and D) n1 latencies. (E and F) p1-n1 amplitudes. Like the ABR results, when the latency-intensity and amplitude-intensity functions are normalized for threshold, they nearly overlapped across genotypes. This result suggests that vestibular loss is primarily caused by reduced end-organ sensitivity rather than changes in neural timing or activity. Mean ± SEM are plotted for each point.

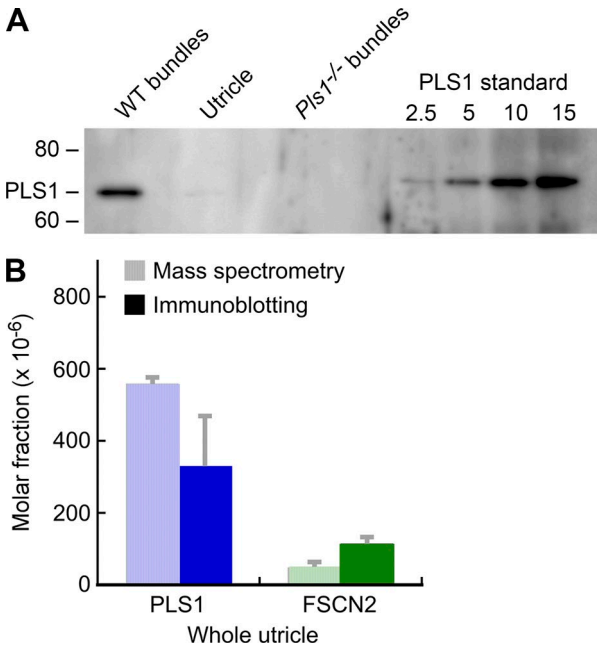

Figure S4. **Quantitation of PLS1 and FSCN2 in whole epithelium by quantitative immunoblotting and MS.** (A) Quantitative immunoblotting example. Samples separated by SDS-PAGE and analyzed by immunoblotting were: wild-type hair bundles (10 ear equivalents), two whole utricles, *Pls1*$^{-/-}$ bundles (10 ear equivalents), and the indicated dilutions of human PLS1 protein (TP306291; Origene). ImageJ was used to obtain the band intensity, and the standards were used to estimate the amount of mouse PLS1. FSCN2 quantitation by quantitative immunoblotting was similar. (B) Comparison of MS and quantitative immunoblotting; the estimated molar abundance (x_n) is indicated. Values for MS were relative molar intensity (i_m) values from Krey et al. (2015). Estimates of the amount of cross-linker estimated by quantitative immunoblotting were divided by the total protein per utricle (45 pmol), which was calculated using a mean molecular mass of 37.3 kD (calculated from the sum of all molecular masses weighted by i_m values for each P23 UTR protein in Krey et al., 2015) and 1.7 ± 0.5 µg total protein per mouse utricle (n = 19). Mean ± SEM are plotted for mass spectrometry and immunoblotting quantitation.

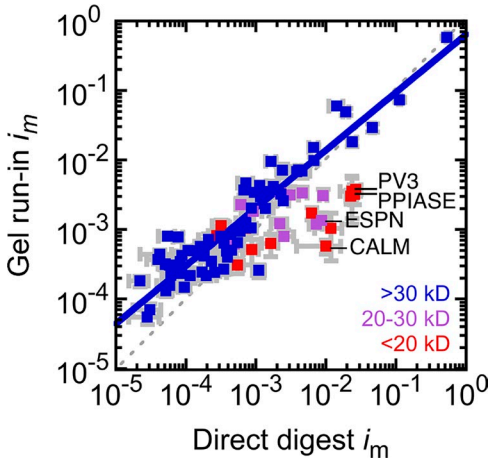

Figure S5. **Comparison of hair-bundle proteins after in-gel digest or direct digestion.** Embryonic day 19–20 chick utricle hair bundles were prepared using in-gel digest or by directly incubating agarose-embedded bundles with trypsin. In either case, peptides were analyzed with an LTQ ion-trap mass spectrometer, and proteins were assembled and quantified using the PAW pipeline (Wilmarth et al., 2009). Relative molar abundances (i_m) for each protein in each experiment were compared; detected proteins were color-coded by their apparent molecular mass as indicated. Note that many of the smallest proteins (<20 kD) were predominantly well to the right of the unity line (dashed line), indicating a higher concentration in the direct digest than in the in-gel digest. In the in-gel digest, proteins can be lost during the initial steps of gel processing; by contrast, in the direct digest approach, no bundle proteins are lost during processing. Mean ± SEM are plotted for each point.

References

Krey, J.F., N.E. Sherman, E.D. Jeffery, D. Choi, and P.G. Barr-Gillespie. 2015. The proteome of mouse vestibular hair bundles over development. *Sci. Data.* 2:150047. http://dx.doi.org/10.1038/sdata.2015.47

Li, A., J. Xue, and E.H. Peterson. 2008. Architecture of the mouse utricle: macular organization and hair bundle heights. *J. Neurophysiol.* 99:718–733. http://dx.doi.org/10.1152/jn.00831.2007

Wilmarth, P.A., M.A. Riviere, and L.L. David. 2009. Techniques for accurate protein identification in shotgun proteomic studies of human, mouse, bovine, and chicken lenses. *J. Ocul. Biol. Dis. Infor.* 2:223–234. http://dx.doi.org/10.1007/s12177-009-9042-6